

Supplementary Information for

A weak luminescent Tb-MOF-based “turn-on” sensor for highly selective and sensitive sensing of anthrax biomarker

Xiao-Yang Zhao, Hui Yang, Wen-Yuan Zhao, Jia Wang, Qi-Shan Yang[□]

School of Chemistry and Chemical Engineering, Inner Mongolia University of Science and Technology, Baotou 014000, China, E-mail: yqs63@sina.com

Table S1. Selected Bond Lengths (Å) and angles (°) of Tb-MOF

Tb-MOF			
Tb(1)-O(10)	2.390(4)	Tb(1)-O(4)	2.382(4)
Tb(1)-O(5)#1	2.341(4)	Tb(1)-O(11)	2.383(5)
Tb(1)-O(7)	2.407(4)	Tb(1)-O(1)	2.308(4)
Tb(1)-O(2)#1	2.386(4)	Tb(1)-C(9)	2.831(6)
Tb(1)-O(8)	2.540(4)		
O(10)-Tb(1)-O(7)	102.42(16)	O(4)-Tb(1)-O(7)	76.62(15)
O(10)-Tb(1)-O(8)	76.16(14)	O(4)-Tb(1)-O(2)#1	76.87(15)
O(10)-Tb(1)-C(9)	90.21(17)	O(4)-Tb(1)-O(8)	69.97(14)
O(5)#1-Tb(1)-O(10)	77.66(14)	O(4)-Tb(1)-O(11)	141.28(18)
O(5)#1-Tb(1)-O(7)	145.64(15)	O(4)-Tb(1)-C(9)	70.44(16)
O(5)#1-Tb(1)-O(2)#1	79.50(14)	O(11)-Tb(1)-O(10)	72.35(18)
O(5)#1-Tb(1)-O(8)	151.77(14)	O(11)-Tb(1)-O(7)	71.87(19)
O(5)#1-Tb(1)-O(4)	126.55(13)	O(11)-Tb(1)-O(2)#1	141.82(18)
O(5)#1-Tb(1)-O(11)	75.63(18)	O(11)-Tb(1)-O(8)	105.92(18)
O(5)#1-Tb(1)-C(9)	162.91(16)	O(11)-Tb(1)-C(9)	89.3(2)
O(7)-Tb(1)-O(8)	52.49(14)	O(1)-Tb(1)-O(10)	146.09(16)
O(7)-Tb(1)-C(9)	25.94(16)	O(1)-Tb(1)-O(5)#1	77.20(14)
O(2)#1-Tb(1)-O(10)	74.36(16)	O(1)-Tb(1)-O(7)	86.17(15)
O(2)#1-Tb(1)-O(7)	134.20(15)	O(1)-Tb(1)-O(2)#1	122.32(14)
O(2)#1-Tb(1)-O(8)	83.45(14)	O(1)-Tb(1)-O(8)	131.02(13)
O(2)#1-Tb(1)-C(9)	109.05(17)	O(1)-Tb(1)-O(4)	76.36(14)
O(8)-Tb(1)-C(9)	26.58(15)	O(1)-Tb(1)-O(11)	79.61(18)
O(4)-Tb(1)-O(10)	137.46(15)	O(1)-Tb(1)-C(9)	108.43(17)
C(13)-O(10)-Tb(1)	126.9(4)	C(5)-O(5)-Tb(1)#1	135.2(4)
C(9)-O(7)-Tb(1)	96.4(3)		

Symmetry Codes: #1= -x+1,-y+1,-z+1

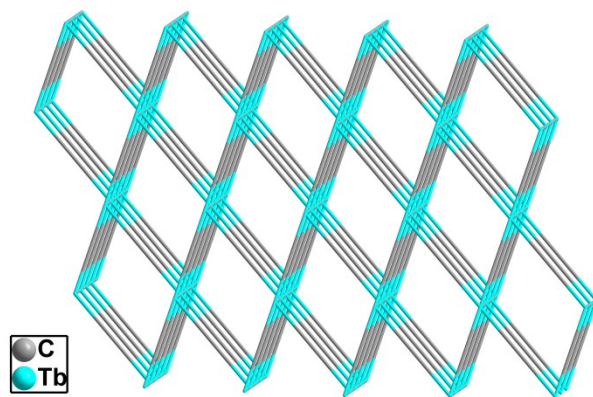


Fig. S1. Tb-MOF with 3D *pcu* topological grid structure.

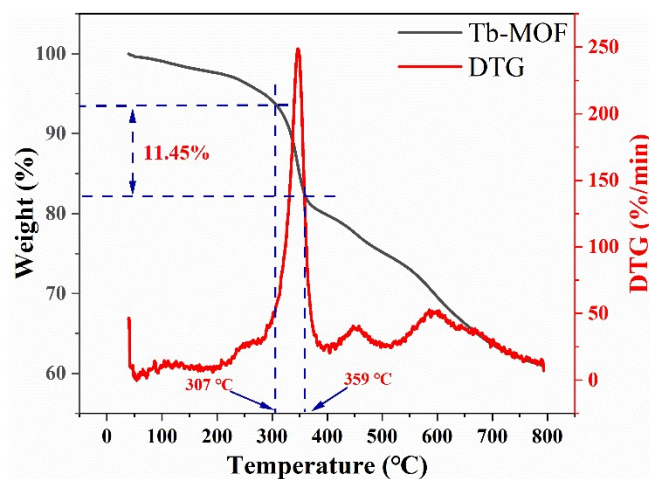


Fig. S2. The thermal gravimetric (TGA) and derivative thermogravimetry (DTG) curves of Tb-MOF

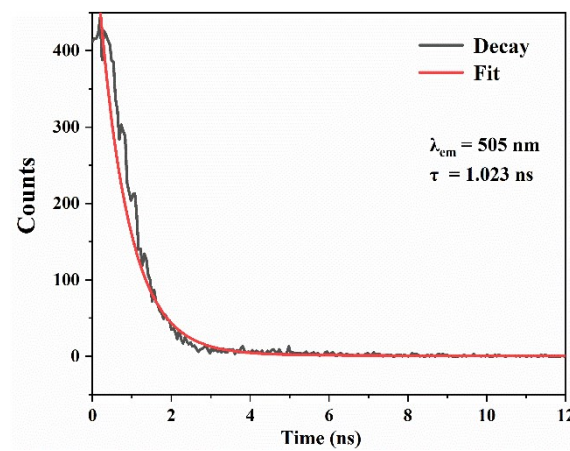


Fig. S3. Fluorescence lifetime decay curve of Tb-MOF at room temperature ($\lambda_{\text{em}} = 505 \text{ nm}$).

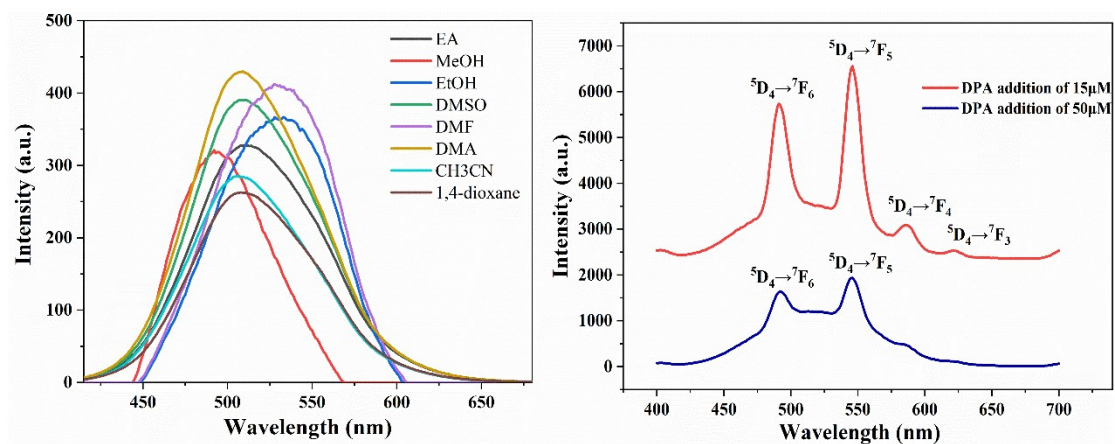


Fig. S4. (a) Fluorescence spectra of Tb-MOF in various solvents; (b) Fluorescence curves of Tb-MOF with DPA concentration at 15 and 50 μM .

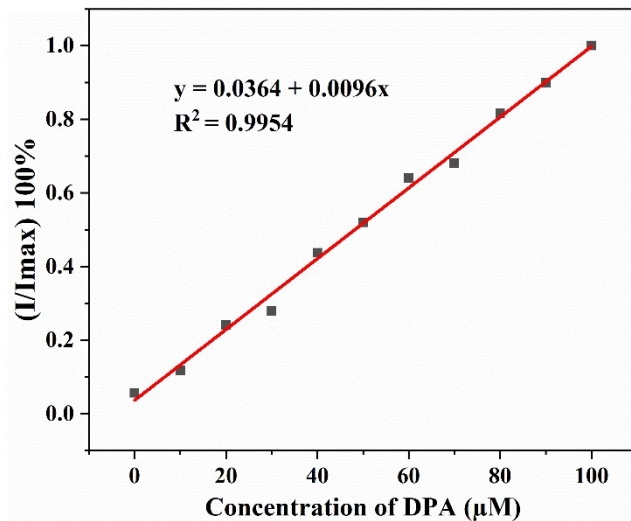


Fig. S5. Linear relationships between the fluorescence intensity (I/I_{\max}) and concentration of DPA.

Table S2. Comparison of literature reports for MOFs as sensors of DPA

MOF	Detection limit	Medium	Reference
Tb-MOF	2.4 μM	H_2O	This work
$\text{Tb}^{3+}\text{-PV}$	5 μM	H_2O	36
R6H@Eu(BTC)	4.5 μM	EtOH	37
$\text{NH}_2\text{-MOF-76(Eu)}$	3.8 μM	EtOH	7
$\text{Tb}_{0.875}\text{Eu}_{0.125}\text{-Hddb}$	19.1 μM	H_2O	38

R6G/Eu-CdS@ZIF-8	67 nM	H ₂ O	39
Eu _{0.1} Tb _{0.9} (BDC)(H ₂ O)Cl	2.27 μM	HEPES	40

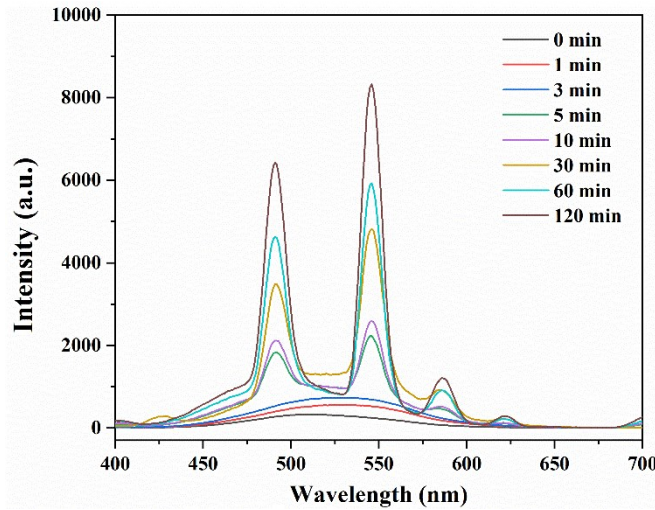


Fig. S6. Emission spectra of Tb-MOF in aqueous solution under DPA (100 μM) at various time intervals.

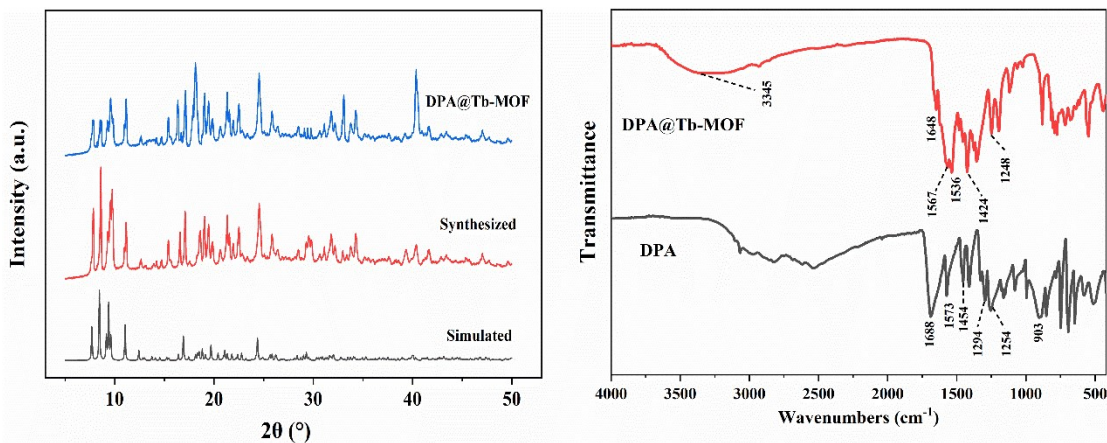


Fig. S7. (a) PXRD spectrum of DPA interacting with Tb-MOF (b) FT-IR spectra of Tb-MOF and DPA@Tb-MOF

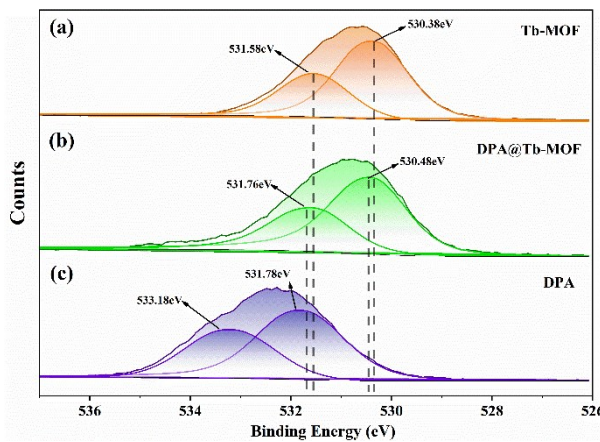


Fig. S8. The XPS spectra for the O1s region of (a) Tb-MOF, (b) DPA@Tb-MOF and (c) DPA.

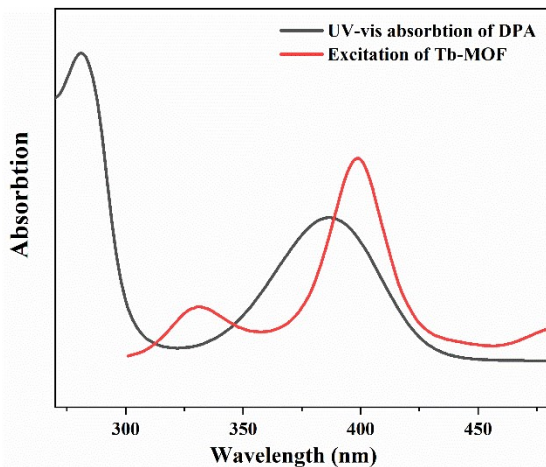


Fig. S9. The excitation spectra of Tb-MOF and the UV-vis absorption spectra of DPA.